Environmental Science & Technology Letters

pubs.acs.org/journal/estlcu

Letter

Application of Single-Particle ICP-MS to Determine the Mass Distribution and Number Concentrations of Environmental Nanoparticles and Colloids

Muammar Mansor,* Sören Drabesch, Timm Bayer, Anh Van Le, Ankita Chauhan, Johanna Schmidtmann, Stefan Peiffer, and Andreas Kappler

Cite This: *Environ. Sci. Technol. Lett.* 2021, 8, 589−595

Read Online

ACCESS | Metrics & More | Article Recommendations | Supporting Information

ABSTRACT: Analyzing the elemental compositions and size distributions of nanoparticles, colloids, and their aggregates in environmental samples represents a key task in understanding contaminant, substrate, and nutrient cycling. Single-particle ICP-MS (spICP-MS) is a high-throughput method that is capable of providing the elemental mass of thousands of particles within minutes. The challenge, however, lies in data analysis and interpretation, especially for complex environmental samples. Here we present successful applications of spICP-MS for environmental samples. We first analyzed the homoaggregation behavior of synthetic microplastic and magnetite (abiogenic and biogenic) nanoparticles. The measured distribution of aggregate mass was described as a function of the number of primary particles/aggregate (N_{pp}). In tandem with dynamic light scattering data, differences in aggregates' compactness (primary particles per nanometer) between samples can be determined. Second, we showed how sequential elemental analysis allows evaluation of the mobility of a toxic arsenic metalloid and its inferred association with colloidal Fe(III) (oxyhydr)oxides. Finally, we investigated the composition of heterogeneous iron−carbon-rich colloidal flocs, highlighting distinct colloidal Fe and C distributions and C/Fe ratios between samples from different permafrost thawing stages. On the basis of our results, we provide guidelines for successful sample preparation and promising future spICP-MS opportunities and applications with environmental samples.

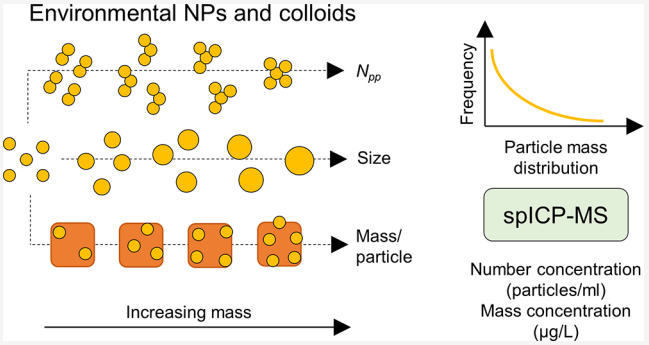

INTRODUCTION

Nanoparticles (NPs, ≤100 nm in diameter) and colloids (≤1000 nm) constitute a highly dynamic environmental pool of elements with a wide continuum of size, reactivity, aggregation, and transport properties. Natural NPs have always been part of the Earth's biogeochemical cycling, while engineered and incidental NPs are increasingly being released to the environment due to anthropogenic activities.[1] Our understanding of particle-driven processes is limited by the analytical techniques at our disposal. Electron microscopy is the standard technique for providing mineralogical and elemental information at the single-particle level but suffers from the high cost, time, and effort needed to translate this information to the whole particle population, as well as artifacts during sample preparation. In contrast, sequential filtration (coupled to subsequent elemental/mineralogical analyses) provides population-level information about particles separated into discrete size classes but fails to treat them as a continuum of size and reactivity. Field-flow fractionation can also separate particles on the basis of their properties (e.g., size), but separation parameters are highly sample-specific.[2] A combination of all of these techniques is ideal for characterizing NPs and colloids, but a gap in our understanding of how to combine the information gained from single particle up to the population level remains.

Single-particle inductively coupled plasma mass spectrometry (spICP-MS) has the potential to become the method of choice to fill this technical gap. In spICP-MS, single particles are channeled to the instrument and detected as separate pulses in a time-resolved mode.[3,4] The intensity of each pulse is proportional to the element mass per particle and can be converted to particle size given prior knowledge on the particle's density, shape, and element mass fraction (Figure 1). Sample preparation is comparatively simple, often requiring only dilutions, and thousands of particles can be analyzed within minutes. Simultaneous information is obtained at the

Received: April 27, 2021
Revised: May 26, 2021
Accepted: May 26, 2021
Published: May 28, 2021

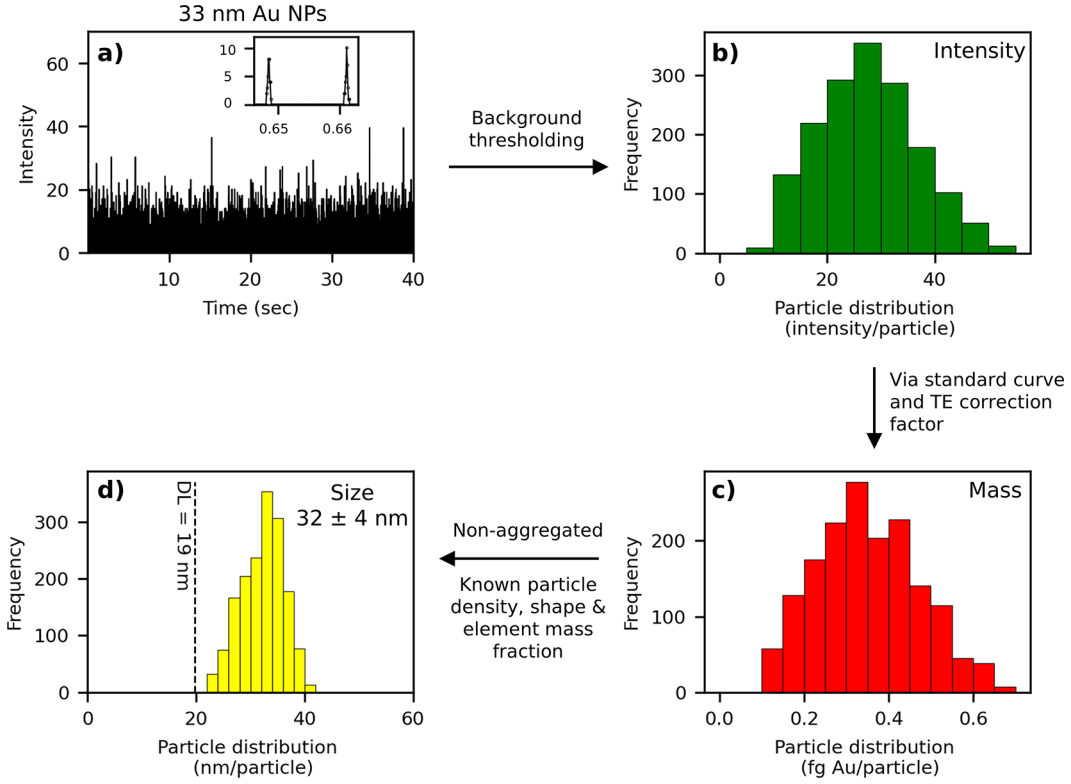

Figure 1. Illustration of data processing steps for spICP-MS. (a) The gold (Au) nanoparticle (NP) standard is analyzed in single-particle mode, yielding a time series consisting of pulses corresponding to particle detection events. The inset shows two adjoining pulses within a time frame of ~0.02 s, with a background intensity of 0. (b) After the application of background thresholding (typically mean + three standard deviations), intensities corresponding to particle pulses are collected to generate a histogram. (c) Particle intensities are converted to the element mass per particle using a standard curve from dissolved elements and a transport efficiency (TE) correction factor (to account for the different efficiency for the detection of dissolved elements vs particles). The masses can be summed to obtain the total mass or concentration in a sample. (d) Mass distribution can be converted to particle size distribution if the particles are non-aggregated and if the particle density, shape, and metal mass fraction are known.

single-particle level (particle mass distribution) as well as the population level (particle number and mass concentration). However, the use of spICP-MS for characterization of natural colloids has lagged behind its use for engineered NPs,[5−7] largely due to the inherent complexity of the former. spICP-MS is also limited to the analysis of one element per particle, but elemental association can be inferred by sequential elemental analysis of the same sample. The lack of element- and size-specific reference materials is another challenge, although so far commonly used calibration techniques are suitable for most particles[5,8,9] (except for selenium NPs[10]).

Here we detail approaches to characterizing and interpreting spICP-MS data from environmental samples to facilitate the adoption of this technique. We present examples ranging from relatively simple aggregation of lab-synthesized particles (microplastics and abiogenic vs biogenic magnetite nanoparticles) to particle-facilitated mobilization of the toxic metalloid arsenic and characterization of iron−carbon-rich colloids from a thawing permafrost.

MATERIALS AND METHODS

All samples were analyzed in time-resolved analysis mode on an Agilent 7900 ICP-MS instrument (Agilent Technologies, Santa Clara, CA) with a RF power of 1550 V and a sampling depth of 8 mm. Samples and standards were prepared and measured as detailed in Tables S1 and S2, with results from standards listed in Table S3. Acid and water rinses were monitored between samples to ensure no carryover. The transport efficiency (TE) was determined daily by comparing the median intensity of 50 nm Au NPs to that of dissolved Au standards using the particle mass method, which is less susceptible to dilution errors compared to the particle number method.[3,11] Over six separate days, the TE was comparable and averaged 0.037 ± 0.001. Masses of ^{12}C, ^{27}Al, ^{56}Fe, ^{75}As, or ^{197}Au were monitored using an integration time of 0.1 ms, an acquisition time of 40−60 s, and a sample flow rate of 0.466 mL/min in either NoGas (argon only) or Gas mode (helium flow of 1 mL/min). Sequential analysis with a time gap of 10 s between elements was employed for multielement analysis of the same sample. Data analysis was performed via a custom Python script following the approaches of Pace et al.[11] and as described in detail in SI Data Analysis. Lower detection limits with increasing element mass were observed (Table S2), consistent with previous studies.[12,13]

RESULTS AND DISCUSSION

Example 1: Aggregation of Microplastic Beads and Magnetite Nanoparticles. Aggregation of nanoparticles and colloids greatly affects their reactivity (surface area loss) and mobility (settling velocity).[14] With spICP-MS, particle mass distribution can be directly measured as a parameter to quantify the state of aggregation. An example is presented for the aggregation of synthetic polystyrene microplastic beads, which affects the sedimentation and mobilization of micro-

https://doi.org/10.1021/acs.estlett.1c00314
Environ. Sci. Technol. Lett. 2021, 8, 589−595

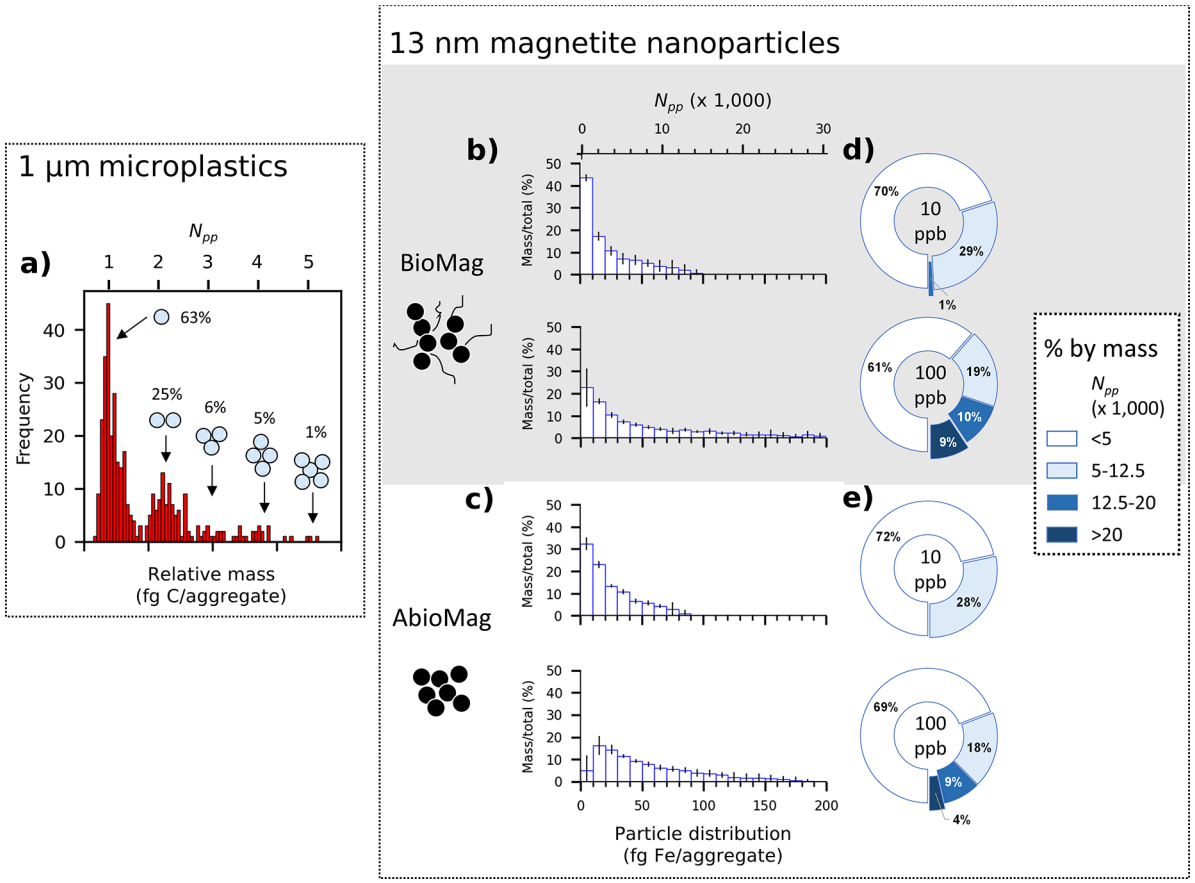

Figure 2. Examples of the usage of spICP-MS to quantify particle aggregation. (a) Frequency-based particle distribution (femtograms of C per aggregate) of unsonicated 1 μm microplastic beads. The detected particles cluster on the basis of their relative masses, which varies according to their corresponding N_{pp} [number of primary particles per aggregate (formula in SI Data Analysis)]. The use of the term N_{pp} allows for the description of the particle distribution based on their masses, remaining true to the parameter actually measured by spICP-MS. The percentages of each aggregate can be quantified on the basis of their relative detection frequencies with a typical reproducibility of <1%. Mass-based particle distribution of (b) biogenic (BioMag) and (c) abiogenic (AbioMag) magnetite NPs at 10 and 100 ppb total Fe. The *y*-axis is converted from number frequency to mass (percent mass within a histogram bin relative to total particle mass in the sample). Error bars correspond to standard deviations from triplicate measurements. (d and e) Mass-based percentages of the magnetite aggregates. Most of the particle masses are contributed by aggregates with N_{pp} values of <5000 (these include masses of particles smaller than the spICP-MS detection limit, assuming no dissolved Fe in the samples). The mass distribution changes depending on the total NP concentration (10 vs 100 ppb Fe) and the sample type (BioMag vs AbioMag).

plastics in aquatic systems.[15,16] Here we introduce the term N_{pp} (number of primary particles per aggregate), which can be obtained by dividing the mass of the measured aggregate (determined via spICP-MS) to the mass of the primary particle [calculable for particles of known size and composition (SI Data Analysis)]. Figure 2a shows that particle signals consisting of isolated microplastic beads (N_{pp} = 1) and aggregates composed of five beads (N_{pp} = 5) were readily distinguished on the basis of their relative masses. Furthermore, the number frequency of each aggregate can be summed and compared to yield their relative frequencies and aggregation pattern. The combination of spICP-MS with ongoing work on microplastic aggregation holds promise for providing new insights on their fate in the environment.[9,17−19]

This approach was further developed through the analysis of ∼13 nm NPs of abiogenic and biogenic magnetite.[20−22] The detection limit for spICP-MS is 0.9 fg of Fe/particle, which means that only aggregates larger than 140 N_{pp} can be detected. Panels b and c of Figure 2 show that magnetite aggregates with up to 30000 N_{pp} were detectable. Due to the smaller sizes, the separation of signals for nanoparticle aggregates was not as clear as for the larger microplastics, but differences in aggregation patterns were still distinguishable. Analyzing the same samples at higher particle concentrations led to the formation of larger aggregates and a more positively skewed particle distribution, because the level of aggregation increases with the total number of primary particles in the suspension.[23,24] Between samples, biogenic magnetite was observed to form larger aggregates compared to abiogenic magnetite at the same concentration. This result was consistent with measurements of the hydrodynamic diameter (D_H) via dynamic light scattering; biogenic magnetite displayed a D_H of 3671 ± 670 nm (n = 9) compared to a smaller D_H of 1567 ± 192 nm (n = 8) for abiogenic magnetite.

By combining measurements of N_{pp} from spICP-MS and D_H from DLS,[25] we can calculate the compaction factor (CF, number of primary particles per nanometer) of a sample:

$$CF = N_{pp}/D_H \quad (1)$$

We determined the CF for biogenic magnetite to be 2−6 times smaller than that of abiogenic magnetite, depending on the measurement dilutions and statistics used to describe

https://doi.org/10.1021/acs.estlett.1c00314
Environ. Sci. Technol. Lett. 2021, 8, 589−595

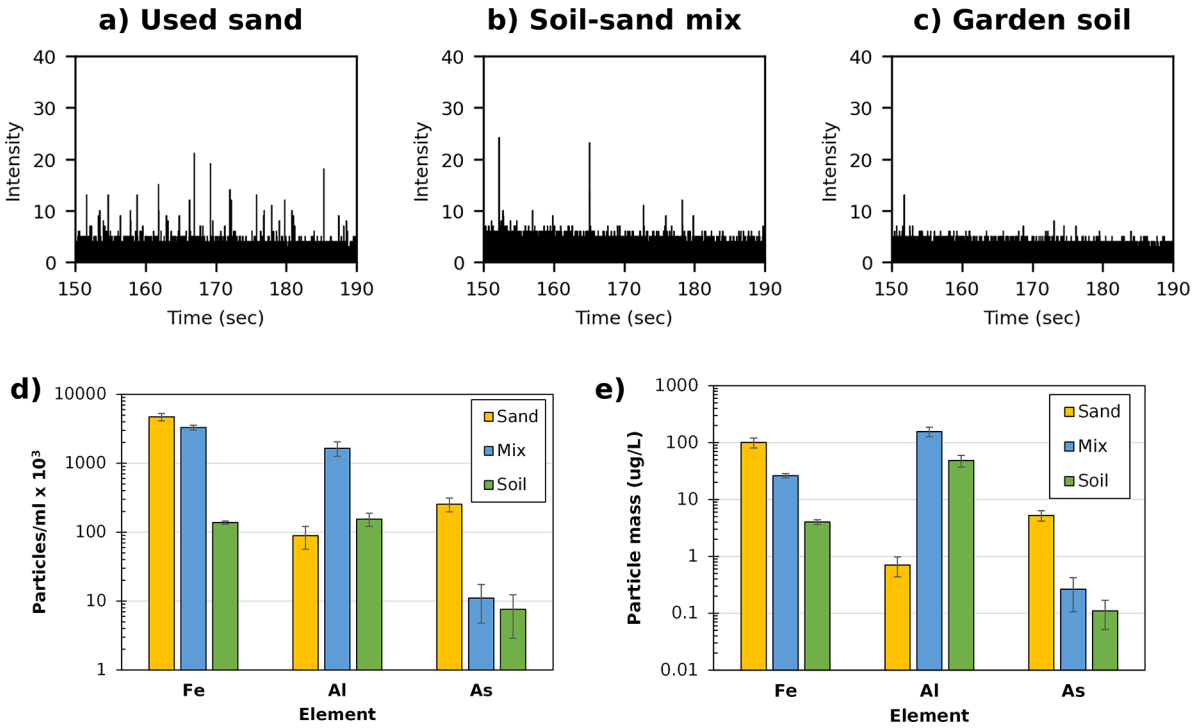

Figure 3. Example of spICP-MS usage to quantify colloidal contaminant mobilization. (a−c) Raw spICP-MS time series for arsenic (As) in used As-rich sand filters (left), a sand/soil mix (middle), and uncontaminated garden soil (right). The used sand filters show elevated levels of colloidal As. (d and e) Particle number concentrations (left) and particle mass concentrations (right) of Fe-, Al-, and As-containing colloids. The two parameters show the same trend between samples but with different relative values depending on the particle number frequency in each mass histogram bin, highlighting the need to compare both number and mass concentrations side by side. Error bars represent standard deviations from measurements of three separate microcosm bottles.

skewed particle distributions (Table S4). The lower CF values indicated that biogenic magnetite formed less compact aggregates than abiogenic magnetite. Overall, the data suggest that biogenic magnetite aggregation was enhanced via bridging by associated organic matter, but they were not packed as tightly as in the case of abiogenic magnetite. This in turn would affect the particle reactivity, which depends on the degree of reactive sites lost due to the decrease in surface area (as well as organic matter coverage) upon aggregation. Note, however, that CF values are dependent on the sample concentrations used for both DLS (parts per million level required due to lower sensitivity) and spICP-MS (parts per billion level) but can be applied to compare different samples as long as the same concentrations are used.

Example 2: Colloid-Facilitated Mobilization of Arsenic Contaminant from Used Sand Filters. In Asia, household sand-based filters are used regularly to treat arsenic-contaminated groundwater for drinking. Oxidation of dissolved Fe(II) in the sand filter results in the formation of solid-phase Fe(III) (oxyhydr)oxides that sequester toxic As and remove it from solution.[26] After being used up, the contaminated sand filter material is often dumped in the backyard garden, thus potentially acting as a point source that will channel As back into the pore water or enter the human food chain.

Our ongoing research has shown limited release of dissolved As from the used sand even as Fe(III) reduction occurs extensively in anoxic microcosms (Table S1). However, we noticed that the microcosms also produced colloids that remain stably suspended in solution for weeks. We therefore investigated through spICP-MS if colloid-facilitated mobilization of As could be an important mechanism for As release, similar to the case in acid mine drainage.[27]

Colloids from three microcosm samples were analyzed: As-rich used sand, uncontaminated garden soil, and a 1:1 mixture of the two. The results were stark. As-containing colloids were detectable and most abundant from the used sand (∼50), followed by the sand/soil mix (∼10), while very low As-containing colloids were detected in uncontaminated soil (≤2; comparable to the H_2O blank) (Figure 3a−c). After accounting for dilution, colloids from used sand were found to contain ∼10^5 As-containing particles per milliliter with a collective mass of ∼10 μg/L As, close to the World Health Organization's drinking water limit for dissolved As (Figure 3d,e). The bioavailability of these colloids is an open question. Nonetheless, this result indicated that colloid-facilitated mobilization of As from used sand could indeed be an important source of contamination.

We sought to understand the particle association of As by monitoring colloidal Fe and Al (Figure 3e,f). The used sand contained a higher level of colloidal Fe but a lower level of colloidal Al than soil and the sand/soil mix. This trend was consistent regardless of whether the particle number or particle mass concentration was used as a comparison metric. Given the concurrent increased Fe and As levels, we hypothesize that As was mobilized in the form of colloidal Fe(III) (oxyhydr)-oxides, consistent with their known associations.[28] Future work using (sub)micrometer visualization of the elemental distribution will help in the evaluation of this hypothesis.

Example 3: Colloidal Fe−Carbon Flocs Released from Thawing Permafrost. Permafrost regions store a significant amount of organic carbon that is becoming increasingly

https://doi.org/10.1021/acs.estlett.1c00314
Environ. Sci. Technol. Lett. 2021, 8, 589−595

bioavailable due to an increasing global temperature.[29] Thawing of permafrost leads to the release of organic carbon that interacts with iron to form Fe−organic-rich aggregates (flocs). These flocs are composed of heterogeneous mixtures of amorphous Fe (oxyhydr)oxides with humic acids, microbial cells, and plant detritus that are likely to be highly reactive and mobile.[30,31] Characterizing these flocs is vital for understanding the role that they will play in greenhouse gas formation and climate change.

We analyzed the flocs collected from an intermediately thawed bog and a fully thawed fen from the Stordalen Mire (Abisko, Sweden). Bog and fen represent two distinct stages of thawing permafrost with different biogeochemical characteristics (e.g., E_h−pH, microbial communities).[32] Figure 4

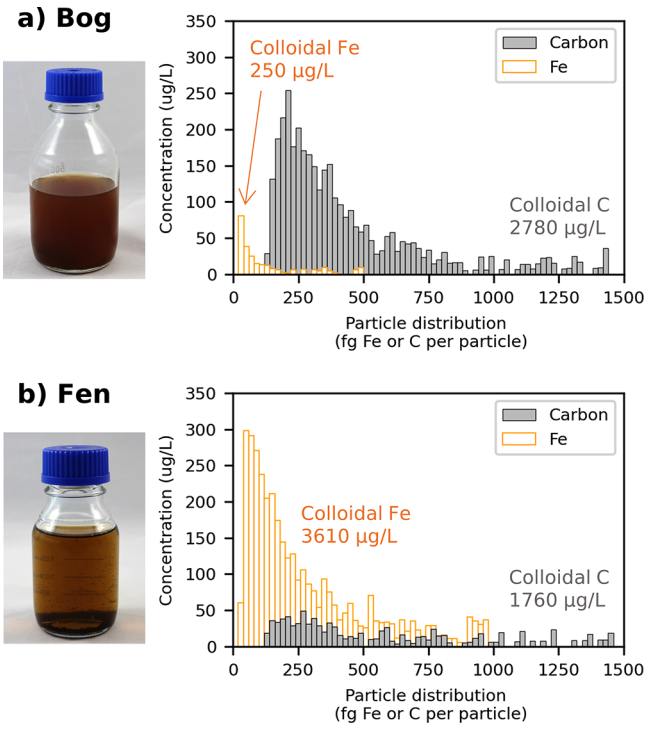

Figure 4. Results of spICP-MS analysis from colloidal Fe−C flocs from (a) bog and (b) fen samples. The *y*-axis shows the colloid concentration (micrograms per liter) by converting from frequency to mass to concentration after correcting for the sample volume analyzed (see SI Data Analysis). The lack of smaller colloidal Fe (<20 fg of Fe/particle) and C particles (<140 fg of C/particles) is not due to their absence but is rather due to the detection limit of spICP-MS. Replicate samples show the same trend even after different treatments (Figure S1).

illustrates the colloidal C and Fe distribution. A significant difference was apparent between the two samples. Flocs from the bog were characterized by high colloidal C and low colloidal Fe concentrations, while flocs from the fen were characterized by low colloidal C (~1.5-fold lower) and high colloidal Fe (~15-fold higher) concentrations. Correspondingly, the total colloidal C/Fe ratio (mass/mass) decreased from 14.3 ± 3.7 (n = 8) to 0.7 ± 0.5 (n = 7; replicates including different treatments in Figure S1) from bog to fen. The increase in the colloidal Fe concentration may be explained by microbial Fe cycling that weathers large particles to form smaller colloidal particles that could be detected by spICP-MS, while the decrease in the colloidal C concentration was consistent with inferred organic C degradation during the bog-to-fen transition.[32] Lower colloidal Fe and C concentrations were also likely present but not detectable due to the detection limit of spICP-MS (Table S2).

Guidelines and Future Opportunities. The presented examples highlight the utility of spICP-MS in providing new insights into particle aggregation, adsorption, and mobilization of toxic elements and their mass distributions in environmental samples. The given examples are only snapshots, and further analysis will undoubtedly provide more information about particle-driven biogeochemical cycling as a function of time or reaction progress. Sample preparation and interpretation are vital for spICP-MS, and here we present several guidelines.

Remove large particles (>5 μm) by filtration, centrifugation, or gravitational settling to avoid clogging in the tubings. When using gravitational settling, always report the container type, sample volume and height, settling time, and sampling depth.

Dilute samples to a particle number concentration of $\leq 10^6$ particles/mL or to low parts per billion levels to reduce coincidence (two particles reaching the plasma at the same time) and particle carryover effects.[3] Optimal dilution for unknown environmental samples can be determined via trial and error. The diluent choice is a compromise between ease of use and minimization of background and elemental interference (MQ H_2O) to maintain an environmentally relevant pH and ionic strength (e.g., filtered environmental water).

Consciously select your mixing methods. Sonication for 5−10 min followed by brief mixing by inversion is recommended for analysis of irreversibly bonded aggregates. Weaker mixing methods such as hand shaking and gas bubbling can be used to analyze weakly bonded agglomerates.

Choose the appropriate sample container, tubings, and reagents to minimize background and adsorptive losses. Reagents can be filtered beforehand to remove colloids. Fe and Al colloids are especially common in blank reagents, but they can be statistically removed by conservative background thresholding.

Variants of spICP-MS are increasingly finding environmental applications.[7] Single-cell ICP-MS has been used successfully to quantify the metal content of single cells.[33,34] Recent development of dual-element spICP-MS and time-of-flight (TOF) spICP-MS can identify elemental association at the single-particle level.[35−38] We expect spICP-MS to be an essential tool in environmental research in upcoming years.

■ ASSOCIATED CONTENT

Supporting Information

The Supporting Information is available free of charge at https://pubs.acs.org/doi/10.1021/acs.estlett.1c00314.

Thorough overview of the data analysis steps (PDF)

Preparation of the sample and standards (Table S1), measurement details and detection limits for each element (Table S2), size and particle number concentration of standards (Table S3), determination of compaction factors from associated D_H and N_{pp} values of magnetite (Table S4), and spICP-MS results of bog and fen samples after treatment with N_2 degassing or sonication (Figure S1) (PDF)

https://doi.org/10.1021/acs.estlett.1c00314
Environ. Sci. Technol. Lett. 2021, 8, 589−595

AUTHOR INFORMATION

Corresponding Author

Muammar Mansor − *Geomicrobiology, Center for Applied Geosciences, University of Tuebingen, 72076 Tuebingen, Germany;* orcid.org/0000-0001-7830-650X; Email: muammar.muammar-bin-mansor@uni-tuebingen.de

Authors

Sören Drabesch − *Geomicrobiology, Center for Applied Geosciences, University of Tuebingen, 72076 Tuebingen, Germany*

Timm Bayer − *Geomicrobiology, Center for Applied Geosciences, University of Tuebingen, 72076 Tuebingen, Germany*

Anh Van Le − *Geomicrobiology, Center for Applied Geosciences, University of Tuebingen, 72076 Tuebingen, Germany*

Ankita Chauhan − *Geomicrobiology, Center for Applied Geosciences, University of Tuebingen, 72076 Tuebingen, Germany*

Johanna Schmidtmann − *Department of Hydrology, University of Bayreuth, 95447 Bayreuth, Germany*

Stefan Peiffer − *Department of Hydrology, University of Bayreuth, 95447 Bayreuth, Germany;* orcid.org/0000-0002-8326-0240

Andreas Kappler − *Geomicrobiology, Center for Applied Geosciences, University of Tuebingen, 72076 Tuebingen, Germany;* orcid.org/0000-0002-3558-9500

Complete contact information is available at: https://pubs.acs.org/10.1021/acs.estlett.1c00314

Author Contributions

M.M. adapted the spICP-MS technique with a focus on environmental applications, supported and encouraged by A.K. S.D. provided invaluable support with ICP-MS analysis. A.C., A.V.L., J.S., and T.B. provided samples. T.B. performed zetasizer measurements. All authors contributed to data interpretation and manuscript revisions.

Notes

The authors declare no competing financial interest.

ACKNOWLEDGMENTS

M.M. thanks Jie Xu for initial support in encouraging him to learn new techniques, Jim Ranville and Manuel Montaño for teaching him spICP-MS, Saurav Kumar for building the original Python framework for data analysis, Weinan Leng and Frank Wackenhut for supplying Au NPs, Peter Kühn for supplying noble metal standards, and Christoph Glotzbach for easy access to the ICP-MS instrument. A.C. acknowledges Monique Patzner and Erik Lundin (Abisko Research Station, Abisko, Sweden) for their help in sampling and providing floc samples. The authors acknowledge infrastructural support by the Deutsche Forschungsgemeinschaft (DFG, German Research Foundation) under Germany's Excellence Strategy, cluster of Excellence EXC2124, Project 390838134. This work was supported by the DFG Project 391977956 (SFB 1357) as well as DFG funding provided to AK (KA 1736/66-1, KA 1736/51-1, and KA 1736/48-1 and Cluster of Excellence: EXC 2124: Controlling Microbes to Fight Infection, Tübingen, Germany).

REFERENCES

(1) Hochella, M. F.; Mogk, D. W.; Ranville, J.; Allen, I. C.; Luther, G. W.; Marr, L. C.; McGrail, B. P.; Murayama, M.; Qafoku, N. P.; Rosso, K. M.; Sahai, N.; Schroeder, P. A.; Vikesland, P.; Westerhoff, P.; Yang, Y. Natural, Incidental, and Engineered Nanomaterials and Their Impacts on the Earth System. *Science* **2019**, *363* (6434), 363.

(2) Moens, C.; Waegeneers, N.; Fritzsche, A.; Nobels, P.; Smolders, E. A Systematic Evaluation of Flow Field Flow Fractionation and Single-Particle ICP-MS to Obtain the Size Distribution of Organo-Mineral Iron Oxyhydroxide Colloids. *J. Chromatogr. A* **2019**, *1599*, 203−214.

(3) Montaño, M. D.; Olesik, J. W.; Barber, A. G.; Challis, K.; Ranville, J. F. Single Particle ICP-MS: Advances toward Routine Analysis of Nanomaterials. *Anal. Bioanal. Chem.* **2016**, *408* (19), 5053−5074.

(4) Degueldre, C.; Favarger, P. Y. Colloid Analysis by Single Particle Inductively Coupled Plasma-Mass Spectroscopy: A Feasibility Study. *Colloids Surf., A* **2003**, *217* (1−3), 137−142.

(5) Mozhayeva, D.; Engelhard, C. A Critical Review of Single Particle Inductively Coupled Plasma Mass Spectrometry-A Step towards an Ideal Method for Nanomaterial Characterization. *J. Anal. At. Spectrom.* **2020**, *35* (9), 1740−1783.

(6) Peters, R.; Herrera-Rivera, Z.; Undas, A.; Van Der Lee, M.; Marvin, H.; Bouwmeester, H.; Weigel, S. Single Particle ICP-MS Combined with a Data Evaluation Tool as a Routine Technique for the Analysis of Nanoparticles in Complex Matrices. *J. Anal. At. Spectrom.* **2015**, *30* (6), 1274−1285.

(7) Flores, K.; Turley, R. S.; Valdes, C.; Ye, Y.; Cantu, J.; Hernandez-Viezcas, J. A.; Parsons, J. G.; Gardea-Torresdey, J. L. Environmental Applications and Recent Innovations in Single Particle Inductively Coupled Plasma Mass Spectrometry (SP-ICP-MS). *Appl. Spectrosc. Rev.* **2021**, *56* (1), 1−26.

(8) Montaño, M. D.; Majestic, B. J.; Jämting, Å. K.; Westerhoff, P.; Ranville, J. F. Methods for the Detection and Characterization of Silica Colloids by Microsecond SpICP-MS. *Anal. Chem.* **2016**, *88* (9), 4733−4741.

(9) Laborda, F.; Trujillo, C.; Lobinski, R. Analysis of Microplastics in Consumer Products by Single Particle-Inductively Coupled Plasma Mass Spectrometry Using the Carbon-13 Isotope. *Talanta* **2021**, *221*, 121486.

(10) Jiménez-Lamana, J.; Abad-Álvaro, I.; Bierla, K.; Laborda, F.; Szpunar, J.; Lobinski, R. Detection and Characterization of Biogenic Selenium Nanoparticles in Selenium-Rich Yeast by Single Particle ICPMS. *J. Anal. At. Spectrom.* **2018**, *33* (3), 452−460.

(11) Pace, H. E.; Rogers, N. J.; Jarolimek, C.; Coleman, V. A.; Higgins, C. P.; Ranville, J. F. Determining Transport Efficiency for the Purpose of Counting and Sizing Nanoparticles via Single Particle Inductively Coupled Plasma Mass Spectrometry. *Anal. Chem.* **2011**, *83* (24), 9361−9369.

(12) Lee, S.; Bi, X.; Reed, R. B.; Ranville, J. F.; Herckes, P.; Westerhoff, P. Nanoparticle Size Detection Limits by Single Particle ICP-MS for 40 Elements. *Environ. Sci. Technol.* **2014**, *48* (17), 10291−10300.

(13) Laborda, F.; Gimenez-Ingalaturre, A. C.; Bolea, E.; Castillo, J. R. About Detectability and Limits of Detection in Single Particle Inductively Coupled Plasma Mass Spectrometry. *Spectrochim. Acta, Part B* **2020**, *169*, 105883.

(14) Hotze, E. M.; Phenrat, T.; Lowry, G. V. Nanoparticle Aggregation : Challenges to Understanding Transport and Reactivity in the Environment. *J. Environ. Qual.* **2010**, *39* (6), 1909−1924.

(15) Li, Y.; Wang, X.; Fu, W.; Xia, X.; Liu, C.; Min, J.; Zhang, W.; Crittenden, J. C. Interactions between Nano/Micro Plastics and Suspended Sediment in Water: Implications on Aggregation and Settling. *Water Res.* **2019**, *161*, 486−495.

(16) Michels, J.; Stippkugel, A.; Lenz, M.; Wirtz, K.; Engel, A. Rapid Aggregation of Biofilm-Covered Microplastics with Marine Biogenic Particles. *Proc. R. Soc. London, Ser. B* **2018**, *285* (1885), 20181203.

(17) Alimi, O. S.; Farner Budarz, J.; Hernandez, L. M.; Tufenkji, N. Microplastics and Nanoplastics in Aquatic Environments: Aggrega-

tion, Deposition, and Enhanced Contaminant Transport. *Environ. Sci. Technol.* **2018**, *52* (4), 1704−1724.
(18) Oriekhova, O.; Stoll, S. Heteroaggregation of Nanoplastic Particles in the Presence of Inorganic Colloids and Natural Organic Matter. *Environ. Sci.: Nano* **2018**, *5* (3), 792−799.
(19) Bolea-Fernandez, E.; Rua-Ibarz, A.; Velimirovic, M.; Tirez, K.; Vanhaecke, F. Detection of Microplastics Using Inductively Coupled Plasma-Mass Spectrometry (ICP-MS) Operated in Single-Event Mode. *J. Anal. At. Spectrom.* **2020**, *35* (3), 455−460.
(20) Sundman, A.; Vitzthum, A. L.; Adaktylos-Surber, K.; Figueroa, A. I.; van der Laan, G.; Daus, B.; Kappler, A.; Byrne, J. M. Effect of Fe-Metabolizing Bacteria and Humic Substances on Magnetite Nanoparticle Reactivity towards Arsenic and Chromium. *J. Hazard. Mater.* **2020**, *384*, 121450.
(21) Pearce, C. I.; Qafoku, O.; Liu, J.; Arenholz, E.; Heald, S. M.; Kukkadapu, R. K.; Gorski, C. A.; Henderson, C. M. B.; Rosso, K. M. Synthesis and Properties of Titanomagnetite ($Fe_{3-x}Ti_xO_4$) Nanoparticles: A Tunable Solid-State Fe(II/III) Redox System. *J. Colloid Interface Sci.* **2012**, *387* (1), 24−38.
(22) Byrne, J. M.; Telling, N. D.; Coker, V. S.; Pattrick, R. A. D.; Van Der Laan, G.; Arenholz, E.; Tuna, F.; Lloyd, J. R. Control of Nanoparticle Size, Reactivity and Magnetic Properties during the Bioproduction of Magnetite by *Geobacter Sulfurreducens*. *Nanotechnology* **2011**, *22* (45), 455709.
(23) Baalousha, M. Aggregation and Disaggregation of Iron Oxide Nanoparticles: Influence of Particle Concentration, PH and Natural Organic Matter. *Sci. Total Environ.* **2009**, *407* (6), 2093−2101.
(24) Vikesland, P. J.; Rebodos, R. L.; Bottero, J. Y.; Rose, J.; Masion, A. Aggregation and Sedimentation of Magnetite Nanoparticle Clusters. *Environ. Sci.: Nano* **2016**, *3* (3), 567−577.
(25) Li, Z.; Shakiba, S.; Deng, N.; Chen, J.; Louie, S. M.; Hu, Y. Natural Organic Matter (NOM) Imparts Molecular-Weight-Dependent Steric Stabilization or Electrostatic Destabilization to Ferrihydrite Nanoparticles. *Environ. Sci. Technol.* **2020**, *54*, 6761−6770.
(26) Nitzsche, K. S.; Weigold, P.; Lösekann-Behrens, T.; Kappler, A.; Behrens, S. Microbial Community Composition of a Household Sand Filter Used for Arsenic, Iron, and Manganese Removal from Groundwater in Vietnam. *Chemosphere* **2015**, *138*, 47−59.
(27) Gomez-Gonzalez, M. A.; Bolea, E.; O'Day, P. A.; Garcia-Guinea, J.; Garrido, F.; Laborda, F. Combining Single-Particle Inductively Coupled Plasma Mass Spectrometry and X-Ray Absorption Spectroscopy to Evaluate the Release of Colloidal Arsenic from Environmental Samples. *Anal. Bioanal. Chem.* **2016**, *408* (19), 5125−5135.
(28) Wallis, I.; Prommer, H.; Berg, M.; Siade, A. J.; Sun, J.; Kipfer, R. The River−Groundwater Interface as a Hotspot for Arsenic Release. *Nat. Geosci.* **2020**, *13* (4), 288−295.
(29) Estop-Aragonés, C.; Cooper, M. D. A.; Fisher, J. P.; Thierry, A.; Garnett, M. H.; Charman, D. J.; Murton, J. B.; Phoenix, G. K.; Treharne, R.; Sanderson, N. K.; Burn, C. R.; Kokelj, S. V.; Wolfe, S. A.; Lewkowicz, A. G.; Williams, M.; Hartley, I. P. Limited Release of Previously-Frozen C and Increased New Peat Formation after Thaw in Permafrost Peatlands. *Soil Biol. Biochem.* **2018**, *118*, 115−129.
(30) Zak, D.; Gelbrecht, J. The Mobilisation of Phosphorus, Organic Carbon and Ammonium in the Initial Stage of Fen Rewetting (a Case Study from NE Germany). *Biogeochemistry* **2007**, *85* (2), 141−151.
(31) Pokrovsky, O. S.; Shirokova, L. S.; Kirpotin, S. N.; Audry, S.; Viers, J.; Dupré, B. Effect of Permafrost Thawing on Organic Carbon and Trace Element Colloidal Speciation in the Thermokarst Lakes of Western Siberia. *Biogeosciences* **2011**, *8* (3), 565−583.
(32) Patzner, M. S.; Mueller, C. W.; Malusova, M.; Baur, M.; Nikeleit, V.; Scholten, T.; Hoeschen, C.; Byrne, J. M.; Borch, T.; Kappler, A.; Bryce, C. Iron Mineral Dissolution Releases Iron and Associated Organic Carbon during Permafrost Thaw. *Nat. Commun.* **2020**, *11* (1), 1−11.
(33) Amor, M.; Tharaud, M.; Gélabert, A.; Komeili, A. Single-Cell Determination of Iron Content in Magnetotactic Bacteria: Implications for the Iron Biogeochemical Cycle. *Environ. Microbiol.* **2020**, *22* (3), 823−831.
(34) Gomez-Gomez, B.; Corte-Rodríguez, M.; Perez-Corona, M. T.; Bettmer, J.; Montes-Bayón, M.; Madrid, Y. Combined Single Cell and Single Particle ICP-TQ-MS Analysis to Quantitatively Evaluate the Uptake and Biotransformation of Tellurium Nanoparticles in Bacteria. *Anal. Chim. Acta* **2020**, *1128*, 116−128.
(35) Montaño, M. D.; Badiei, H. R.; Bazargan, S.; Ranville, J. F. Improvements in the Detection and Characterization of Engineered Nanoparticles Using SpICP-MS with Microsecond Dwell Times. *Environ. Sci.: Nano* **2014**, *1* (4), 338−346.
(36) Bevers, S.; Montaño, M. D.; Rybicki, L.; Hofmann, T.; von der Kammer, F.; Ranville, J. F. Quantification and Characterization of Nanoparticulate Zinc in an Urban Watershed. *Front. Environ. Sci.* **2020**, *8*, 1−16.
(37) Praetorius, A.; Gundlach-Graham, A.; Goldberg, E.; Fabienke, W.; Navratilova, J.; Gondikas, A.; Kaegi, R.; Günther, D.; Hofmann, T.; Von Der Kammer, F. Single-Particle Multi-Element Fingerprinting (SpMEF) Using Inductively-Coupled Plasma Time-of-Flight Mass Spectrometry (ICP-TOFMS) to Identify Engineered Nanoparticles against the Elevated Natural Background in Soils. *Environ. Sci.: Nano* **2017**, *4* (2), 307−314.
(38) Naasz, S.; Weigel, S.; Borovinskaya, O.; Serva, A.; Cascio, C.; Undas, A. K.; Simeone, F. C.; Marvin, H. J. P.; Peters, R. J. B. Multi-Element Analysis of Single Nanoparticles by ICP-MS Using Quadrupole and Time-of-Flight Technologies. *J. Anal. At. Spectrom.* **2018**, *33* (5), 835−845.

https://doi.org/10.1021/acs.estlett.1c00314
Environ. Sci. Technol. Lett. 2021, 8, 589−595